

Enhancement of the tidal disruption event rate in galaxies with a nuclear star cluster: from dwarfs to ellipticals

Hugo Pfister,^{1,2} Marta Volonteri,³ Jane Lixin Dai^{2,1} and Monica Colpi^{4,5}

¹*DARK, Niels Bohr Institute, University of Copenhagen, Blegdamsvej 17, DK-2100 Copenhagen, Denmark*

²*Department of Physics, The University of Hong Kong, Pokfulam Road, Hong Kong, China*

³*Sorbonne Université, CNRS, UMR7095, Institut d’Astrophysique de Paris, 98bis boulevard Arago, F-75014, Paris, France*

⁴*Dipartimento di Fisica G. Occhialini, Università degli Studi di Milano–Bicocca, Piazza della Scienza 3, I-20126 Milano, Italy*

⁵*National Institute of Nuclear Physics INFN, Milano - Bicocca, Piazza della Scienza 3, 20126 Milano, Italy*

Accepted XXX. Received YYY; in original form ZZZ

ABSTRACT

We compute the tidal disruption event (TDE) rate around local massive black holes (MBHs) with masses as low as $2.5 \times 10^4 M_\odot$, thus probing the dwarf regime for the first time. We select a sample of 37 galaxies for which we have the surface stellar density profile, a dynamical estimate of the mass of the MBH, and 6 of which, including our Milky Way, have a resolved nuclear star cluster (NSC). For the Milky Way, we find a total TDE rate of $\sim 10^{-4} \text{ yr}^{-1}$ when taking the NSC in account, and $\sim 10^{-7} \text{ yr}^{-1}$ otherwise. TDEs are mainly sourced from the NSC for light ($< 3 \times 10^{10} M_\odot$) galaxies, with a rate of few 10^{-5} yr^{-1} , and an enhancement of up to 2 orders of magnitude compared to non-nucleated galaxies. We create a mock population of galaxies using different sets of scaling relations to explore trends with galaxy mass, taking into account the nucleated fraction of galaxies. Overall, we find a rate of few 10^{-5} yr^{-1} which drops when galaxies are more massive than $10^{11} M_\odot$ and contain MBHs swallowing stars whole and resulting in no observed TDE.

Key words: transients: tidal disruption events – galaxies: dwarf – galaxies: nuclei – galaxies: bulges

1 INTRODUCTION

When a star passes sufficiently close to a massive black hole (MBH), it can get accreted. For solar-type stars and MBHs with mass up to $\sim 10^8 M_\odot$, the star is not swallowed whole, but it is tidally perturbed and destroyed, with a fraction of its mass falling back on to the MBH causing a bright flare, known as a tidal disruption event (TDE; Hills 1975; Rees 1988). As transient luminous events, TDEs are excellent candidates to discover low luminosity dormant intermediate mass black holes in dwarf galaxies (Greene et al. 2019). Moreover, as stars are not subject to feedback, which prevents MBH growth in dwarf galaxies (Dubois et al. 2014; Trebitsch et al. 2018), repeated TDEs, and subsequent accretion of stellar debris, could be a mechanism to “grow” these intermediate mass black holes (Rees 1988; Alexander & Bar-Or 2017).

From an observational perspective, with a handful of TDEs observed, in the X-ray (e.g. Auchettl et al. 2017) where most of the emission is produced, or in the optical/UV (e.g. van Velzen et al. 2011; Gezari et al. 2012; van

Velzen et al. 2020) for which surveys can cover a large area of the sky, it is now possible to estimate the TDE rate per galaxy. Unfortunately, the number of TDEs is still too low to undoubtedly conclude on the precise value of the rate, and different groups, with different samples and methods find different values: $10^{-5} \text{ yr}^{-1} \text{ gal}^{-1}$ (van Velzen et al. 2011), $10^{-4} \text{ yr}^{-1} \text{ gal}^{-1}$ (van Velzen 2018; Auchettl et al. 2018), with probably a dependence on the properties of galaxies (French et al. 2016; Law-Smith et al. 2017; Graur et al. 2018), and with some galaxies possibly having a TDE rate as high as 10^{-1} yr^{-1} (Tadhunter et al. 2017).

From a theoretical perspective, the most efficient way to bring stars close enough to the MBH to be disrupted is 2-body interactions (Lightman & Shapiro 1977; Merritt 2013). Wang & Merritt (2004) find that the TDE rate in an isothermal sphere surrounding a MBH lying on the $M_\bullet - \sigma$ relation (Kormendy & Ho 2013) is:

$$\Gamma = 6.5 \times 10^{-4} \text{ yr}^{-1} \left(\frac{M_\bullet}{10^6 M_\odot} \right)^{-0.25}, \quad (1)$$

where M_\bullet is the mass of the MBH. Stone & Metzger (2016) using a subsample of 144 observed galaxies from Lauer et al. (2007) for which the density profile is available, hence break-

* Sophie and Tycho Brahe Fellow; hugo.pfister@nbi.ku.dk

ing the assumption of the isothermal sphere, find similar rates. Note that the assumption of the central MBH lying on the $M_\bullet - \sigma$ relation is still made.

These two works suggest that lighter MBHs, *i.e.* MBHs in dwarf galaxies, should exhibit a larger rate of TDEs. In addition, the Λ CDM paradigm predicts that dwarf galaxies are the most numerous in our Universe (Bullock & Boylan-Kolchin 2017). All this suggests that most TDEs should come from intermediate mass black holes. This is not what is observed, with a clear drop of the detected number of TDEs for MBHs with masses lower than $\sim 10^6 M_\odot$ (Wevers et al. 2019). However, we remind that the works of Stone & Metzger (2016) and Wang & Merritt (2004) assume that the central MBH lies on the $M_\bullet - \sigma$ relation, which is well constrained for MBHs with masses larger than $\sim 10^6 M_\odot$, but may break down in the dwarf regime (Greene et al. 2019).

In addition, none of these previous works take into account that some galaxies may harbour a nuclear star cluster (NSC). The environment in the center of these galaxies greatly differ from those in non-nucleated galaxies. For example, we show in Fig. 1 the total density profile (thick dashed lines) as well as the bulge/NSC (thick/thin solid lines) decomposition of the dwarf galaxy NGC 205 (blue) and Circinus (orange). These profiles are made using observed Sérsic (Sérsic 1968) decomposition (see §2.2) from Nguyen et al. (2018); Davis et al. (2019) and Pechetti et al. (2019). In the absence of NSC, the central density in the dwarf NGC 205 would be up to 4 orders of magnitude lower. Not only the enhancement is lower in Circinus, but the fraction of nucleated galaxies is lower at higher mass (Sánchez-Janssen et al. 2019). The extreme density found in NSCs is known to speed up the formation of binary BHs due to more efficient dynamical friction and stellar scattering (*e.g.* Biava et al. 2019; Ogiya et al. 2020), but also to boost the TDE rate (Mastrobuono-Battisti et al. 2014; Aharon et al. 2016; Arca-Sedda & Capuzzo-Dolcetta 2017). All this suggests that contributions of NSCs in the dwarf regime should play a major role.

In this paper, we estimate the TDE rate for a sample of 37 galaxies (§3) and for a mock catalog built using a set of scaling relations (§4). For these two samples, (*i*) some MBHs have masses as low as few $10^4 M_\odot$ allowing us to study the TDE rate in the dwarf regime; (*ii*) we relax the assumption that MBHs lie exactly on the $M_\bullet - \sigma$ relation; (*iii*) some galaxies have a nuclear star cluster, allowing us to study the relative contribution of this component compared with the one of the bulge; and (*iv*) we remove MBHs with mass larger than $10^8 M_\odot$ that swallow stars whole and result in no TDE.

2 TDE RATE

In this Section, we explain how we estimate the TDE rate (§2.1) given a density profile (§2.2), we also show how our method agrees with previous results (§2.3).

2.1 Estimate of the TDE rate

We adopt a similar approach to Pfister et al. (2019) to estimate the TDE rate. A spherical density profile $\rho(r)$ with a central MBH is provided as an input to PHASEFLOW

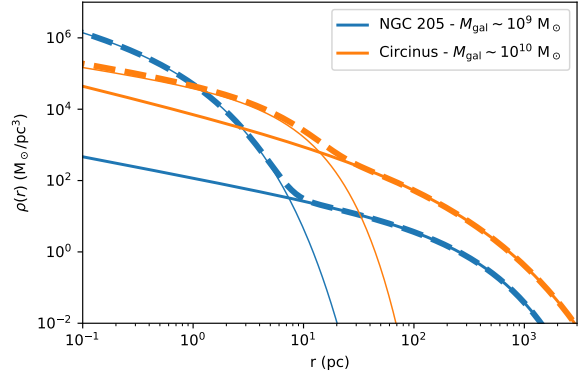


Figure 1. Density of the dwarf NGC 205 (blue) and Circinus (orange). The total density is shown with thick dashed lines, the density of the bulge with thick solid lines and the one of the NSC with thin solid lines. All quantities are shown as a function of the distance to the center of the galaxy.

(Vasiliev 2017, 2019), which computes the following quantities:

- the stellar distribution function $f(E)$, which is further assumed to be ergodic, obtained through the Eddington inversion (Binney & Tremaine 1987). $E = v^2/2 + \phi(r)$ is the energy per unit mass, r and v are respectively the distance to the center and relative speed, and ϕ is the galactic gravitational potential;
- the energy density function $N(E) = 4\pi^2 L_c^2(E)f(E)P(E)$ (Merritt 2013). $L_c(E)$ and $P(E)$ represent respectively the circular angular momentum and radial period of stars with energy E ;
- the loss cone filling factor $q(E)$ (Eq. (13a) from Vasiliev 2017);
- the loss-cone boundary \mathcal{R}_{LC} (Eq. (13b) from Vasiliev 2017);
- the orbit-averaged diffusion coefficient μ (Eq. (13c) from Vasiliev 2017);

With this information, we can infer the TDE flux per unit energy (Eq. (16) from Stone & Metzger (2016), Eq. (14) from Vasiliev (2017), Eq. (8) from Pfister et al. (2019)):

$$\frac{\partial \Gamma}{\partial E} = \frac{q(E) \mathcal{R}_{LC}}{(q(E)^2 + q(E)^4)^{1/4} + \ln(1/\mathcal{R}_{LC})} \frac{N(E)}{P(E)}, \quad (2)$$

which can be integrated to obtain the TDE rate Γ in units of disruptions per year per galaxy.

Note that, although PHASEFLOW can handle different types of stars, with different masses (m_\star) and radii (r_\star), we make the assumption that all stars are solar-like, *i.e.* $m_\star = M_\odot$ and $r_\star = R_\odot$. Stone & Metzger (2016) have shown that this only affects the TDE rate by a factor of ~ 2 .

2.2 Density profiles

Surface density profiles are often (*e.g.* Lauer et al. 2007; Sánchez-Janssen et al. 2019) fitted with a Sérsic profile (Sérsic 1968) which depends on 3 parameters: the mass of the structure M_\star , the Sérsic index n , and the effective radius

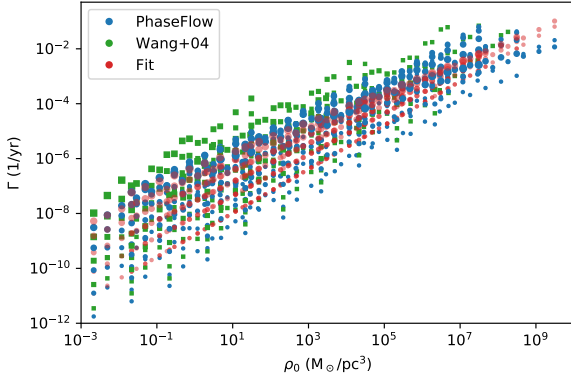


Figure 2. TDE rate as a function of ρ_0 (normalisation of the profile, see Eq. (6)). We show the results of PHASEFLOW (blue), of Eq. (37) of Wang & Merritt (2004) (green) as well as the fit of Eq. (7) (red).

R_{eff} ¹. It has been shown by Prugniel & Simien (1997) and Márquez et al. (2000) that the underlying three dimensional density profile, which we will refer to as the Prugniel profile throughout this paper, is well approximated by:

$$\rho(r) = \rho_0 \left(\frac{r}{R_{\text{eff}}} \right)^{-p} e^{-b(r/R_{\text{eff}})^{1/n}} \quad (3)$$

$$p = 1 - \frac{0.6097}{n} + \frac{0.05563}{n^2} \quad (4)$$

$$b = 2n - \frac{1}{3} + \frac{0.009876}{n} \quad (5)$$

$$\rho_0 = \frac{M_\bullet}{4/3\pi R_{\text{eff}}^3} \times 0.13e^{1.82n} \text{ (see Appendix A).} \quad (6)$$

Our strategy is therefore the following: for a given structure, *i.e.* a galaxy, a bulge, or a NSC, with surface density fitted with a Sérsic profile, we reconstruct the associated three dimensional Prugniel density profile (Eq. (3-6)) and add a central MBH with mass M_\bullet . From this, the TDE rate can be estimated as explained in §2.1.

2.3 Test cases and a simple fit to the TDE rate

To test our method, we build a mock catalog of Sérsic structures, from light NSCs to elliptical galaxies, with a central MBH (see values of M_\star , n , R_{eff} and M_\bullet in Table 1). For each of these structures, we compute the TDE rate with PHASEFLOW. We show the value of the TDE rate as a function of ρ_0 as obtained through this method in Fig. 2 (blue circles). We chose ρ_0 instead of n , M_\star , R_{eff} or M_\bullet because a clear trend arises, confirming that TDEs are more likely to be found in massive (large M_\star), compact (small R_{eff}) and steep (large n) structures (see Eq. (6) for the dependence of ρ_0 on M_\star , n and R_{eff}).

For comparison with previous results, we show (green squares) the TDE rate as estimated by Eq. (37) of Wang & Merritt (2004), assuming a power law density profile

¹ We parametrize the Sérsic profile so that the effective radius is equal to the half-light radius.

$\rho(r) = \rho_0(r/R_{\text{eff}})^{-p}$, which matches with a Prugniel density profile at $r \ll R_{\text{eff}}$ and taking care to remove the cases where the assumptions of Wang & Merritt (2004) are not fulfilled. Specifically, Wang & Merritt (2004) assume that the critical radius, r_{crit} , corresponding to the radius at which the full and the empty loss cone fluxes are equals (Syer & Ulmer 1999), is much smaller than than the influence radius, corresponding to the radius at which the enclosed mass of stars equals the one of the MBH. As Wang & Merritt (2004) also provide an expression for r_{crit} (Eq. (36) of their paper), we can verify this assumption and show only galaxies which fulfill this criterion. Fig. 2 shows that the results of Wang & Merritt (2004) and our approach using a deprojected Sérsic profile and PHASEFLOW are in excellent agreement.

Ideally, one would want to compute the TDE rate given the observed properties of the structures (M_\star , n , R_{eff}) and the central MBH (M_\bullet), without having to go through PHASEFLOW. The variation of the TDE rate with ρ_0 suggests a power law dependency, with the normalization and the logarithmic slope depending on the mass of the MBH. Using a simple least-squares fit, we find the following expression:

$$\Gamma = 10^{-13} \text{ yr}^{-1} \log_{10}^7 \left(\frac{M_\bullet}{M_\odot} \right) \left(\frac{\rho_0}{M_\odot \text{ pc}^{-3}} \right)^{1-0.05 \log_{10}(M_\bullet/M_\odot)}, \quad (7)$$

with the results shown in red in Fig. 2. In practice, in the following, as the number of objects will be small, we will be able to use of PHASEFLOW for all the structures. We note, however, that for a galaxy for which M_\star , n , R_{eff} and M_\bullet are known this is a rapid way of obtaining an estimate of the TDE rate.

3 APPLICATION TO REAL GALAXIES

In this Section, we apply the technique described in §2.1 to real galaxies to obtain the TDE rate. We describe the data we use in §3.1 and give our results in §3.2.

3.1 Data

3.1.1 “Unresolved” galaxies

Davis et al. (2019) published a list of 40 galaxies (including the Milky Way) hosting a MBH, for which they provide M_\star, bulge , n_{bulge} , $R_{\text{eff,bulge}}$ of the bulge and a dynamical estimate of M_\bullet .

3.1.2 “Resolved” galaxies

Similarly to Biava et al. (2019), we use the data of Nguyen et al. (2018) who published a high-resolution study of four galaxies hosting a MBH. For all of their galaxies, they provided the Sérsic quantities n_{bulge} , $M_{\star, \text{bulge}}$, $R_{\text{eff,bulge}}$ of the bulge, the mass of the MBH M_\bullet , as well as the Sérsic quantities n_{NSC} , $M_{\star, \text{NSC}}$, $R_{\text{eff,NSC}}$ of the central NSC. In addition, the recent paper of Pechetti et al. (2019) provides additional Sérsic fits for 29 NSCs, 2 of which belongs to galaxies (Circinus and NGC 5055) included in the sample of Davis et al. (2019).

Quantity	Values	Details
$M_\star (M_\odot)$	$[10^6, 10^{11}]$ Logarithmically spaced by 1.	The lower bound has been chosen to match that of NSCs in which the MBH can reside (Nguyen et al. 2018), the upper bound matches the mass of elliptical galaxies.
n	$[1, 5]$ Linearly spaced by 0.5.	X
$R_{\text{eff}} (\text{pc})$	$[1, 10^2] \text{ pc}$ if $M_\star \leq 10^7$ $[10, 10^3] \text{ pc}$ if $M_\star \in [10^8, 10^9] M_\odot$ $[10^2, 10^4] \text{ pc}$ if $M_\star \geq 10^{10} M_\odot$ Logarithmically spaced by 1.	Chosen to match, within a factor of 10, the typical value found by Dabringhausen et al. (2008).
$M_\bullet (M_\odot)$	$[10^4, M_\star/100] M_\odot$ Logarithmically spaced by 1.	X

Table 1. Parameters used to construct our mock-catalog as well as their values. We end up with 567 mock Sérsic structures with a central MBH.

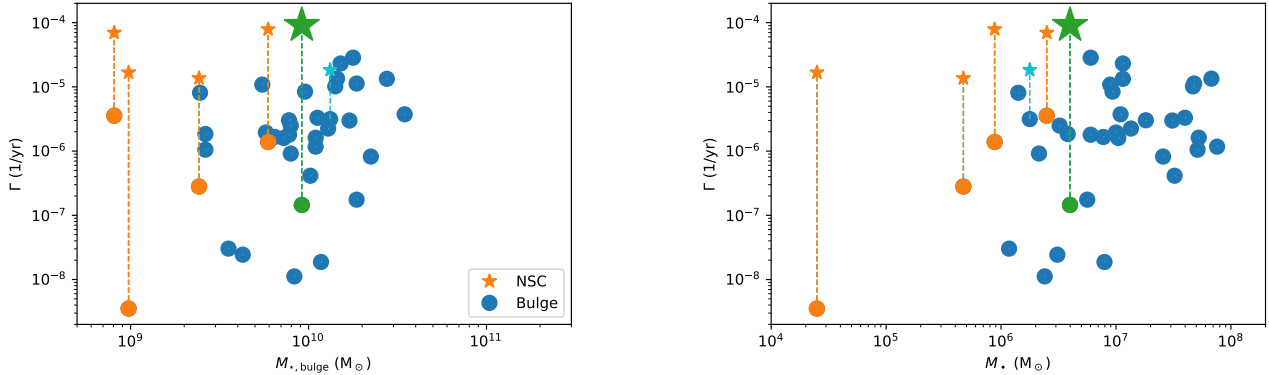


Figure 3. **Left:** TDE rate as a function of the mass of the bulge. **Right:** TDE rate as a function of the mass of the MBH. In both cases we show the TDE rate sourced from the bulge (circles) which can be interpreted as the TDE rate one would infer using “low resolution observations”, and from the NSC (stars). Colors indicate where the data come from (see text).

3.1.3 The Milky Way

Particular care is taken for the Milky Way. Davis et al. (2019) provides the Sérsic parameters for the bulge. Regarding the NSC, we fit the observed luminosity profile of the inner pc of our Galaxy (Fig. 9 of Schödel et al. 2018) with a Sérsic profile. We obtain $(R_{\text{eff,NSC}}/\text{pc}, n_{\text{NSC}}) \sim (6, 2)$. We choose $M_{\star, \text{NSC}} = 4.4 \times 10^7 M_\odot$ so that the density at 1 pc (0.1 pc) is $1.6 \times 10^5 M_\odot \text{ pc}^{-3}$ ($2.2 \times 10^6 M_\odot \text{ pc}^{-3}$) and the mass within 1 pc is $1.3 \times 10^6 M_\odot$, in agreement with the value given in Table 3 of Schödel et al. (2018).

We remove galaxies for which the mass of the MBH is larger than $10^8 M_\odot$, in order to take into account that no TDE would be seen in this situation. This reduces the “observed” sample to 37 galaxies, 6 of which, including our Milky Way, have a resolved NSC. For all these galaxies we use the method described in §2.1 to obtain the TDE rate. For the 6 galaxies with a resolved NSC, we compute separately the TDE rate for stars in the bulge and stars in the NSC. This allows us to study the relative contribution of

each component, and the total TDE rate is simply obtained summing the TDE rate from all components.

This sample is smaller than the one used by Stone & Metzger (2016) to perform a similar analysis, but (i) all the galaxies we consider have a dynamical estimate of the MBH mass, and we do not need to assume it lies on the $M_\bullet - \sigma$ (or equivalently the $M_\bullet - M_{\star, \text{bulge}}$) relation (Kormendy & Ho 2013); (ii) we removed MBHs for which no TDE would be seen; (iii) some of our galaxies have a resolved NSC; and (iv) we extend the analysis to the dwarf galaxy regime, of crucial importance for both TDEs and gravitational wave studies with LISA.

3.2 Rates

We show in Fig. 3 the TDE rate generated by stars in the bulge (circles) and, for galaxies which have a NSC, the TDE rate generated by stars in the NSC (stars) as a function of the mass of the bulge (left panel) and of the MBH (right panel). The different colors indicate where we obtained the data: Nguyen et al. (2018) in orange; Davis et al. (2019) in

dark blue; [Pechetti et al. \(2019\)](#) in light blue and the Milky Way using the NSC of [Schödel et al. \(2018\)](#) in green.

We begin by discussing the TDE rates originating from stars in bulges (circles), which we interpret as the TDE rate one would infer using a density profile obtained with “low resolution observations”. We find a large scatter, with TDE rates that differ by ± 2 dex at fixed bulge/MBH mass. Overall, the TDE rate increases with the bulge (MBH) mass up to few $10^{10} M_\odot$ (few $10^6 M_\odot$) where it plateaus at its maximum value of few 10^{-5} yr^{-1} .

However, this does not take into account the presence of NSCs, which can enhance the TDE rate by orders of magnitude, as shown by the star symbols. Consider for instance the Milky Way, according to [Davis et al. \(2019\)](#) and [Schödel et al. \(2018\)](#), the mass of the central MBH is $4 \times 10^6 M_\odot$ and the bulge/NSC have the following Sérsic properties ($M_{\star,\text{bulge}}/M_\odot, R_{\text{eff,bulge}}/\text{pc}, n_{\text{bulge}}$) $\sim (9.1 \times 10^9, 1040, 1.3)$ and ($M_{\star,\text{NSC}}/M_\odot, R_{\text{eff,NSC}}/\text{pc}, n_{\text{NSC}}$) $\sim (4.4 \times 10^7, 6, 2)$. Using Eq. (6) and Eq. (7), we can estimate the ratio between the TDE rate sourced from the NSC and the bulge, we find about 2,000. As, for a particular galaxy, M_\bullet is fixed, this enhancement of the TDE rate in NSCs is clearly due to the enhancement of ρ_0 (see Eq. (7)). Using PHASEFLOW, we obtain a TDE rate of $9.1 \times 10^{-5} \text{ yr}^{-1}$ (green star) including the NSC and $1.4 \times 10^{-7} \text{ yr}^{-1}$ without it (green circle), resulting in an enhancement of ~ 630 . This example shows how crucial it is to take into account NSCs when they exist.

For the 6 galaxies for which we have the NSC density profiles, we find a total enhancement of the TDE rate when including NSCs varying between 6 (Circinus) to 4800 (NGC 205), with an average at 900. When both the contribution of the bulge and the NSC are included, the mean TDE rate is enhanced by at least 2 orders of magnitude at low bulge ($\sim 10^9 M_\odot$) or MBH ($\sim 10^4 M_\odot$) masses. This results in a constant few 10^{-5} yr^{-1} TDE rate, independent of the mass of the bulge/MBH.

This analysis illustrates how important it is to properly resolve NSCs to have a correct estimate of the TDE rate in the low bulge/MBH mass regime. However, (i) our sample does not contain massive bulges with NSCs, although this is expected (the nucleation fraction has a peak of about 80–100% for $10^9 M_\odot$ galaxies and decreases at lower and higher masses; [Sánchez-Janssen et al. 2019](#)) it would be interesting to know the contribution of NSCs in this regime; and (ii) because it is based on real observations, the size of our sample is limited. In the following §4, we build a realistic mock catalog of galaxies to overcome these issues.

4 UNDERSTANDING THE TREND WITH MOCK CATALOGS

In this Section we perform a similar analysis as in §3 but on a realistic mock catalog. We describe how we build the catalog in §4.1 and give our results in §4.2. This approach is useful in order to make statistical predictions for population of galaxies, and compare with large upcoming observational samples of TDEs.

4.1 Mock catalog

To produce a large realistic sample of galaxies overcoming the issues mentioned in §3.2, we proceed as following 100,000 times:

(i) We draw a galaxy mass M_{gal} from a log-uniform distribution between 10^9 and $10^{12} M_\odot$;

(ii) We compute the mass of the bulge $M_{\star,\text{bulge}}$ fitting the median value of the ratio bulge to total mass (Fig. 3 of [Khochfar et al. 2011](#)):

$$M_{\star,\text{bulge}} = M_{\text{gal}} \times \min \left(1; 10^{-10.1+0.9\log_{10}(M_{\text{gal}}/M_\odot)} \right); \quad (8)$$

(iii) We compute the effective radius of the bulge $R_{\text{eff,bulge}}$ using Eq. (4) of [Dabringhausen et al. \(2008\)](#) (using all objects, read §3.1 of their paper):

$$R_{\text{eff,bulge}} = (2.95 \pm 0.24) \text{ pc} \left(\frac{M_{\star,\text{bulge}}}{10^6 M_\odot} \right)^{0.596 \pm 0.007}; \quad (9)$$

(iv) We compute the mass of the MBH M_\bullet using Eq. (11) of [Davis et al. \(2019\)](#):

$$M_\bullet = 10^{7.24 \pm 0.82} M_\odot \left(\frac{M_{\star,\text{bulge}}}{1.15 \times 10^{10} M_\odot} \right)^{2.44 \pm 0.35}; \quad (10)$$

(v) We compute the Sérsic index of the bulge n_{bulge} using Eq. (12) of [Davis et al. \(2019\)](#):

$$n_{\text{bulge}} = 2.20 \left(\frac{M_\bullet}{10^{7.45 \pm 0.84} M_\odot} \right)^{1/(2.76 \pm 0.70)}; \quad (11)$$

(vi) A random number f is uniformly drawn in [0,1]. If $f < f_{\text{NSC}}(M_{\text{gal}})$, where $f_{\text{NSC}}(M_{\text{gal}})$ is the nuclear fraction for galaxies with mass M_{gal} (Fig. 9 in [Sánchez-Janssen et al. 2019](#)), then we place a NSC and go to step (vii) and further. In the other situation, no NSC is placed. In practice we fitted the nuclear fraction with:

$$f_{\text{NSC}} = 0.9 \times \exp \left[- \left(\frac{\log_{10} \left(\frac{M_{\text{gal}}}{M_\odot} \right) - 8.8}{1.1} \right)^2 \right]; \quad (12)$$

(vii) We compute the mass of the NSC $M_{\star,\text{NSC}}$ using Eq. (6) of [Pechetti et al. \(2019\)](#):

$$M_{\star,\text{NSC}} = 10^{6 \pm 0.13} M_\odot \left(\frac{M_{\text{gal}}}{10^{8.88} M_\odot} \right)^{0.91}; \quad (13)$$

(viii) We compute the effective radius of the NSC $R_{\text{eff,NSC}}$ using Eq. (4) of [Dabringhausen et al. \(2008\)](#) (reported in Eq. (9));

(ix) We compute the Sérsic index n_{NSC} fitting Fig. 8 of [Pechetti et al. \(2019\)](#), we find:

$$\log_{10} n_{\text{NSC}} = (-0.245 \pm 0.094) \log_{10} \left(\frac{M_{\star,\text{NSC}}}{M_\odot} \right) + (2.10 \pm 0.93). \quad (14)$$

For all steps but (ii) and (vi), the fitted parameters used in the relations are drawn from normal distributions $\mathcal{N}(\mu, \sigma)$ with mean μ and standard deviation σ given by the different authors (the $\mu \pm \sigma$ in the Equations). For instance, the parameter a from Eq. (4) in [Dabringhausen et al. \(2008\)](#), used to infer the effective radius of the bulge, is drawn in $\mathcal{N}(2.95, 0.24)$. This is done to take into account the scatter in the scaling relations.

As we assume many relations with their scatter, our

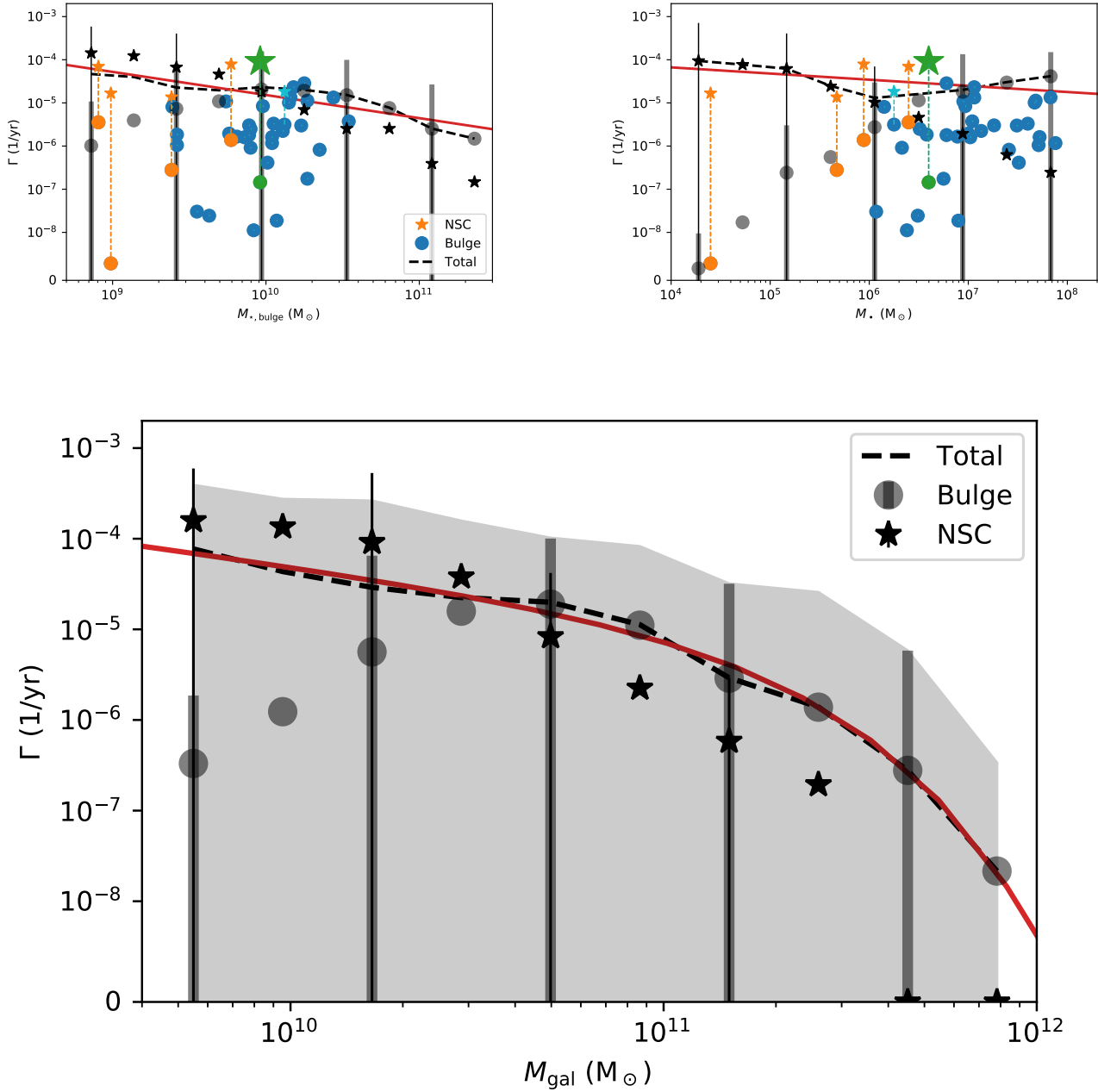


Figure 4. Top left: TDE rate as a function of the mass of the bulge. **Top right:** TDE rate as a function of the mass of the MBH. **Bottom:** TDE rate as a function of the mass of the galaxy. In all cases we show the mean contribution from the bulge (circles) and, for galaxies which have one, from the NSC (stars). When both contributions are included, the mean TDE rate is given by the black dashed line and the fit in red is from Eq. (15-17). Coloured markers represent real galaxies (see §3.1) while black represents the results of our model (see 4.1). Error bars indicate the variance at fixed mass showing that a zero TDE rate is within 1 sigma error at all masses.

method sometime produces “irrealistic” galaxies. In particular, the Sérsic indices could be negative or arbitrarily large. We remove galaxies for which the Sérsic index of the bulge is not in $[0.5, 10]$ (reducing the sample by 2/3) and, among remaining galaxies which have a NSC, we remove those for which the Sérsic index of the NSC is not in $[0.5, 10]$ resulting in $\sim 25,000$ galaxies.

For all galaxies with a MBH less massive than $10^8 M_\odot$,

we compute the TDE rate using the technique described in §2.1. Similarly to §3.1, for galaxies which have a NSC, we compute the TDE rate originating from stars coming from the bulge and the NSC separately in order to study their respective contribution, and the total TDE rate is simply the sum of the two. The TDE rate in galaxies with MBHs more massive than $10^8 M_\odot$ is set to 0 to take into account

that solar like stars would be swallowed whole and no TDE would be seen.

4.2 Results

We show in Fig. 4 the TDE rate generated by stars in the bulge (circles) and, for galaxies which have a NSC, the TDE rate originating from stars in the NSC (stars) as a function of the mass of the bulge (upper left panel), of the MBH (upper right panel) and of the galaxy (lower panel). The mean total TDE rate including all galaxies, even those for which the TDE rate is 0, is shown with the black dashed line. The error bars simply indicate the variance at fixed mass, showing that a zero TDE rate is within a 1 sigma error at all masses. For the two upper panels we also show the TDE rate of the “real” galaxies analyzed in §3.

Overall, both the trend and scatter are well reproduced by our model, with most of the TDE rates of observed galaxies being at less than 1 sigma from the mean value of our model. The three panels show somewhat similar behaviors²: the contribution of stars coming from the bulge increases when the mass of the bulge/MBH/galaxy increases, until it decreases at $3 \times 10^{10} M_\odot/10^8 M_\odot/10^{11} M_\odot$, mostly because MBHs become more massive and stars are swallowed whole resulting in no observed TDEs.

Including TDEs coming from NSCs enhances the total TDE rate by 2/4/2 orders of magnitude for light ($10^9 M_\odot/10^4 M_\odot/5 \times 10^9 M_\odot$) bulges/MBHs/galaxies, however, for more massive objects (bulge/MBH/galaxy more massive than $10^{10} M_\odot/10^7 M_\odot/3 \times 10^{10} M_\odot$), the contribution of NSCs becomes smaller than that of bulges. This is not trivial: it results from the combination of the variation of $R_{\text{eff,bulge}}/R_{\text{eff,NSC}}$ which tend to decrease the TDE rate, and of $n_{\text{bulge}}/M_{\star,\text{bulge}}/M_{\star,\text{NSC}}/n_{\text{NSC}}$ which tend to increase the TDE rate (see Eq. (7) for the dependency the TDE rate with of ρ_0 , and Eq. (6) for the dependency of ρ_0 with the parameters of the bulge/NSC).

On average, the mean total TDE rate (dashed line) is fairly constant with the bulge/MBH/galaxy mass and equal to few 10^{-5} yr^{-1} until $3 \times 10^{10} M_\odot/10^8 M_\odot/10^{11} M_\odot$, when stars are swallowed whole and not tidally disrupted. To be more precise, we use a least-square fit on the mean total TDE rate to obtain:

$$\Gamma = 4 \times 10^{-5} \text{ yr}^{-1} \left(\frac{M_\bullet}{10^6 M_\odot} \right)^{-0.14} \quad (15)$$

$$\Gamma = 10^{-5} \text{ yr}^{-1} \left(\frac{M_{\text{bulge}}}{10^{10} M_\odot} \right)^{-0.54} \quad (16)$$

$$\Gamma = 7 \times 10^{-6} \text{ yr}^{-1} \left(\frac{M_{\text{gal}}}{10^{11} M_\odot} \right)^{-0.55} e^{-\frac{M_{\text{gal}}}{3 \times 10^{11} M_\odot}}. \quad (17)$$

The rates (few 10^{-5} yr^{-1} per galaxy) are in agreement with current observational rates (Donley et al. 2002; van Velzen & Farrar 2014; Auchettl et al. 2018). The logarithmic slope of the trend with MBH mass from $10^4 M_\odot$ to $10^8 M_\odot$, -0.14 , is shallower than that found by Stone & Metzger

² We show the top two panels to overplot our estimated TDE rate from observed galaxies, and the lower panel is useful for comparison with observations for which the mass of the galaxy host is known.

(2016) for their full sample $\ln \Gamma \propto -0.404 \times \ln M_\bullet$. There are two reasons for that. First, if we re-fit the sample of (Stone & Metzger 2016, their Table C1) keeping only MBHs with mass $< 10^8 M_\odot$, as we do in order to consider only observable TDEs, we obtain $\ln \Gamma \propto 0.02 \times \ln M_\bullet$. Furthermore, Stone & Metzger (2016) discuss how fitting separately core and cusp galaxies (Faber et al. 1997) leads to a shallower slope. In our model we have not included core galaxies, which however tend to be more common at the high-mass end, for galaxies with mass³ $> 10^{11} M_\odot$, thus hosting MBHs with mass $> 10^8 M_\odot$, outside the range of interest for TDEs with luminous features.

The distribution of MBH mass of observed TDE flares, although uncertain due to limited sample, peaks at a few $10^6 M_\odot$ (Stone & Metzger 2016; Wevers et al. 2019), while our model predicts an almost flat trend in log space, $\ln \Gamma \propto -0.14 \times \ln M_\bullet$. However, we recall here that we simply compute, for a given bulge/MBH/galaxy mass the average number of stars entering the TDE radius at which they are disrupted. The observability of TDEs however also depends on additional physics such as the overall debris mass supply rate determined by the mass and internal structure of the star, the circularisation efficiency determined by the stellar orbital parameters and black hole mass, the emission mechanism, as well as dust obscuration (Guillochon & Ramirez-Ruiz 2013; Piran et al. 2015; Dai et al. 2015; Roth et al. 2016; Dai et al. 2018; Mockler et al. 2019).

An important point is that we have also assumed that all galaxies harbour a MBH, and while this is probably a good assumption for massive galaxies, it is not the case in the low mass regime, where the occupation fraction is theoretically predicted to decrease (Volonteri et al. 2008). Stone & Metzger (2016) explore the effect of taking into account a MBH occupation fraction that depends on the bulge mass, assuming a one-to-one relation with MBH mass. In this paper we do not include this additional parameter, since its functional form is very uncertain, both theoretically and observationally (Greene et al. 2019). A drop in the TDE rate below our predictions at low galaxy mass would be a hint that the MBH occupation fraction in dwarfs is not 100%.

While the effect of NSCs is negligible in massive ($> 3 \times 10^{10} M_\odot$) galaxies, they form a particularly important component in the dwarf regime (we recall that 90% of $10^9 M_\odot$ galaxies, and more than 50% of $10^8 M_\odot$ galaxies, have a NSC; Sánchez-Janssen et al. 2019), enhancing the TDE rate by few orders of magnitude. We note that Biava et al. (2019), who studied the evolution of lifetime of MBH binaries in the context of gravitational waves for LISA, also find that estimates of the lifetimes of the most massive binaries (in massive galaxies) is not strongly dependent on the details of the central density profile. However, the low mass binary regime is strongly affected by details of the stellar density profile and the presence, or not, of a NSC, with binary lifetimes varying in between 10 Myr, in cases with NSCs, to 100 Gyr in cases without NSCs for $10^5 M_\odot$ binaries. This suggests that, with the hundreds to thousands of TDEs which will be detected with the LSST (van Velzen

³ Most core galaxies have $M_V \lesssim -21$, and we assume a mass-to-light ratio of ~ 10 .

Name	$M_\bullet - M_\star$	$M_{\star, \text{NSC}} - R_{\text{eff, NSC}}$
DD (fiducial)	Davis et al. (2019)	Dabringhausen et al. (2008)
DP	Davis et al. (2019)	Pechetti et al. (2019)
KD	Kormendy & Ho (2013)	Davis et al. (2019)

Table 2. Name of the models and scaling relations used. Our fiducial model is the one described in §4.1

et al. 2011) or eROSITA (Merloni et al. 2012), we will learn about the internal structure of dwarf galaxies, which will be useful in making predictions for gravitational wave detection with LISA.

5 EFFECTS OF UNCERTAINTIES IN THE SCALING RELATIONS

In order to explore trends with MBH, bulge and galaxy mass, we built a mock catalog using a set of scaling relations. However, the physical meaning of these relations is still debated, and different groups, using different samples, find different relations. While we partly took this into account by including the scatter about the relations (see §4.1), we adopt here another approach, using different sets of scaling relations. In particular, we re-do the exact same procedure as in §4.1 but we use other $M_\bullet - M_\star$ and $M_{\star, \text{NSC}} - R_{\text{eff, NSC}}$ relations (see Table 2).

We show in Fig. 5 the TDE rate sourced from the NSC (stars) and from the bulge (circles), for these three models, as a function of the mass of the galaxy (left panel) and of the MBH (right panel). The largest difference comes from changing the scaling relation to obtain $R_{\text{eff, NSC}}$. In particular, when the scaling relation from Pechetti et al. (2019) is used, the inferred TDE rate tends to be larger. This can be easily understood, as the TDE rate scales as $\Gamma \propto \rho_0^\alpha \propto R_{\text{eff, NSC}}^{-3\alpha}$, with $\alpha > 0$ and is a weak function of M_\bullet (see Eq. (7)), and as the scaling relation of Pechetti et al. (2019) tends to predict lower $R_{\text{eff, NSC}}$ at same $M_{\star, \text{NSC}}$ than the scaling relation of Davis et al. (2019).

Overall, the details vary from one model to the other, but always remain within the scatter, and our conclusions remain unaffected.

6 CONCLUSIONS

We have estimated the TDE rate in 37 galaxies for which we have the stellar surface density profile, a dynamical estimate of the mass of the MBH, and 6 of which, including our Milky Way, have a resolved NSC. We also estimated the TDE rate in 25,000 galaxies of a mock catalog built using a set of scaling relations, including the nucleated fraction of galaxies. Our main findings are the following:

- It is necessary to resolve the central part of dwarf galaxies with masses lower than $3 \times 10^{10} M_\odot$ to properly estimate the TDE rate around MBHs with masses lower than $10^6 M_\odot$.

Indeed, these galaxies may harbour a NSC, possibly enhancing the total TDE rate by 1-2 orders of magnitude. Since we assumed an occupation fraction of 100%, a lower TDE rate in dwarfs could be a hint that this fraction is in fact lower in this regime (Stone & Metzger 2016).

- The TDE rate in the Milky Way around Sagittarius A* is predicted to be $9.1 \times 10^{-5} \text{ yr}^{-1}$.

• The TDE rate is roughly constant at few 10^{-5} yr^{-1} for bulges/MBHs/galaxies up to $3 \times 10^{10} M_\odot / 10^8 M_\odot / 10^{11} M_\odot$, after which stars are swallowed whole and not tidally disrupted, resulting in no observed TDEs. This result is independent of the scaling relations used, however, at fixed bulge/MBH/galaxy mass, the scatter in the TDE rate can be as high as ± 2 dex. We also provide fitting formulae giving the mean TDE rate at fixed MBH/bulge/galaxy mass (Eq. (15-17)).

- If the mass of the MBH and the Sérsic parameters of the structure hosting this MBH are known, the TDE rate is well approximated by Eq. (7), where ρ_0 can be obtained through Eq. (6).

Both the TDE rates and the merger rate of MBH binaries detectable as gravitational wave sources depend on the stellar distribution near the MBH(s) and the presence or absence of a NSC (Biava et al. 2019). Future observations of TDEs with the LSST or eROSITA, which will constrain the TDE rate, can then be used to refine our predictions for MBH binary hardening rates and therefore MBH merger rates for LISA. This comparison is subject of an ongoing study.

ACKNOWLEDGMENTS

HP and JD are indebted to the Danish National Research Foundation (DNRF132) and the Hong Kong government (GRF grant HKU27305119) for support. MV thanks Rainer Schödel for help with models of the NSC of the Milky Way. The authors thank the Yukawa Institute for Theoretical Physics at Kyoto University. Discussions during the YITP workshop YITP-T-19-07 on International Molecule-type Workshop "Tidal Disruption Events: General Relativistic Transients" were useful to complete this work.

REFERENCES

Aharon D., Mastrobuono Battisti A., Perets H. B., 2016, *ApJ*, **823**, 137
 Alexander T., Bar-Or B., 2017, *Nature Astronomy*, **1**, 0147
 Arca-Sedda M., Capuzzo-Dolcetta R., 2017, *MNRAS*, **471**, 478
 Auchettl K., Guillochon J., Ramirez-Ruiz E., 2017, *ApJ*, **838**, 149
 Auchettl K., Ramirez-Ruiz E., Guillochon J., 2018, *ApJ*, **852**, 37
 Biava N., Colpi M., Capelo P. R., Bonetti M., Volonteri M., Tam-fal T., Mayer L., Sesana A., 2019, *MNRAS*, **487**, 4985
 Binney J., Tremaine S., 1987, *Galactic Dynamics*, first edn. Princeton Series in Astrophysics, Princeton University Press
 Bullock J. S., Boylan-Kolchin M., 2017, *ARA&A*, **55**, 343
 Dabringhausen J., Hilker M., Kroupa P., 2008, *MNRAS*, **386**, 864
 Dai L., McKinney J. C., Miller M. C., 2015, *ApJ*, **812**, L39
 Dai L., McKinney J. C., Roth N., Ramirez-Ruiz E., Miller M. C., 2018, *ApJ*, **859**, L20
 Davis B. L., Graham A. W., Cameron E., 2019, *ApJ*, **873**, 85
 Donley J. L., Brandt W. N., Eracleous M., Boller T., 2002, *The Astronomical Journal*, **124**, 1308
 MNRAS **000**, 1–9 (2019)

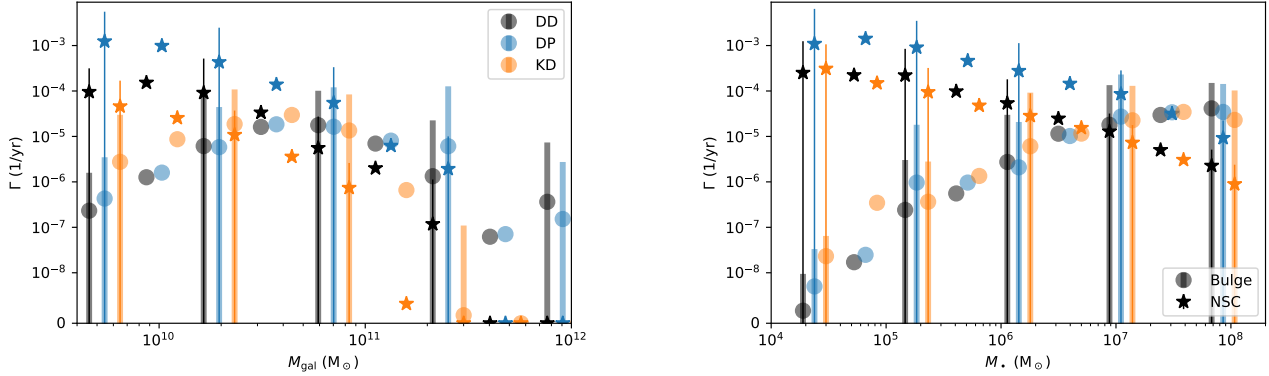


Figure 5. Left: TDE rate as a function of the mass of the galaxy. **Right:** TDE rate as a function of the mass of the MBH. In both cases, contribution from the bulge (circles) and from the NSC (stars) are shown for the 3 models described in Table 2.

Dubois Y., et al., 2014, *MNRAS*, **444**, 1453
 Faber S. M., et al., 1997, *ApJ*, **114**, 1771
 French K. D., Arcavi I., Zabludoff A., 2016, *ApJ*, **818**, L21
 Gezari S., et al., 2012, *Nature*, **485**, 217
 Graur O., French K. D., Zahid H. J., Guillochon J., Mandel K. S., Auchettl K., Zabludoff A. I., 2018, *ApJ*, **853**, 39
 Greene J. E., Strader J., Ho L. C., 2019, arXiv e-prints, p. arXiv:1911.09678
 Guillochon J., Ramirez-Ruiz E., 2013, *ApJ*, **767**, 25
 Hills J. G., 1975, *Nature*, **254**, 295
 Khochfar S., et al., 2011, *MNRAS*, **417**, 845
 Kormendy J., Ho L. C., 2013, *ARAA*, **51**, 511
 Lauer T. R., et al., 2007, *ApJ*, **664**, 226
 Law-Smith J., Ramirez-Ruiz E., Ellison S. L., Foley R. J., 2017, *ApJ*, **850**, 22
 Lightman A. P., Shapiro S. L., 1977, *ApJ*, **211**, 244
 Márquez I., Lima Neto G. B., Capelato H., Durret F., Gerbal D., 2000, *AAP*, **353**, 873
 Mastrobuono-Battisti A., Perets H. B., Loeb A., 2014, *ApJ*, **796**, 40
 Merloni A., et al., 2012, arXiv e-prints, p. arXiv:1209.3114
 Merritt D., 2013, *Dynamics and Evolution of Galactic Nuclei*. Princeton University Press
 Mockler B., Guillochon J., Ramirez-Ruiz E., 2019, *ApJ*, **872**, 151
 Nguyen D. D., et al., 2018, *ApJ*, **858**, 118
 Ogiya G., Hahn O., Mingarelli C. M. F., Volonteri M., 2020, *MNRAS*, **493**, 3676
 Pechetti R., Seth A., Neumayer N., Georgiev I., Kacharov N., den Brok M., 2019, arXiv e-prints, p. arXiv:1911.09686
 Pfister H., Bar-Or B., Volonteri M., Dubois Y., Capelo P. R., 2019, *MNRAS*, p. L87
 Piran T., Svirski G., Krolik J., Cheng R. M., Shiokawa H., 2015, *ApJ*, **806**, 164
 Prugniel P., Simien F., 1997, *AAP*, **321**, 111
 Rees M. J., 1988, *Nature*, **333**, 523
 Roth N., Kasen D., Guillochon J., Ramirez-Ruiz E., 2016, *ApJ*, **827**, 3
 Sánchez-Janssen R., et al., 2019, *ApJ*, **878**, 18
 Schödel R., Gallego-Cano E., Dong H., Nogueras-Lara F., Gallego-Calvente A. T., Amaro-Seoane P., Baumgardt H., 2018, *AAP*, **609**, A27
 Sersic J. L., 1968, *Atlas de Galaxias Australes*
 Stone N. C., Metzger B. D., 2016, *MNRAS*, **455**, 859
 Syer D., Ulmer A., 1999, *MNRAS*, **306**, 35
 Tadhunter C., Spence R., Rose M., Mullaney J., Crowther P., 2017, *Nature Astronomy*, **1**, 0061
 Trebitsch M., Volonteri M., Dubois Y., Madau P., 2018, *MNRAS*, **478**, 5607
 Vasiliev E., 2017, *ApJ*, **848**, 10
 Vasiliev E., 2019, *MNRAS*, **482**, 1525
 Volonteri M., Lodato G., Natarajan P., 2008, *MNRAS*, **383**, 1079
 Wang J., Merritt D., 2004, *ApJ*, **600**, 149
 Wevers T., et al., 2019, *MNRAS*, **487**, 4136
 van Velzen S., 2018, *ApJ*, **852**, 72
 van Velzen S., Farrar G. R., 2014, *ApJ*, **792**, 53
 van Velzen S., et al., 2011, *ApJ*, **741**, 73
 van Velzen S., et al., 2020, arXiv e-prints, p. arXiv:2001.01409

APPENDIX A: AN EXPRESSION FOR ρ_0

Assuming a Prugniel density profile (Eq.(3)), fits for p and b already exist that reproduce a given Sérsic profile in projection. Consequently, only ρ_0 needs to be computed through the total mass as:

$$M_\star = \rho_0 \frac{4}{3} \pi R_{\text{eff}}^3 \times 3 \int_{u=0}^{\infty} u^{2-p} e^{-b u^{1/n}} du. \quad (\text{A1})$$

From this, it is clear that the ratio between ρ_0 and $M_\star/(4/3\pi R_{\text{eff}}^3)$ depends only on n . We estimate this ratio numerically and fit it with an exponential in Fig. A1.

This paper has been typeset from a Te_X/La_Te_X file prepared by the author.

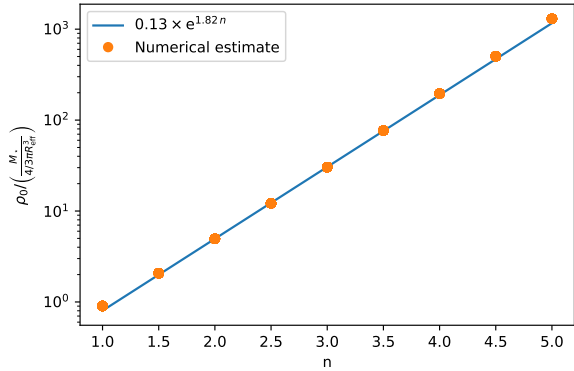


Figure A1. Numerical estimate of $\rho_0 / \left(\frac{M_\star}{4/3\pi R_{\text{eff}}^3} \right)$ (orange circles) as a function of the Sérsic index (n) as well as a fit (blue line). The agreement is excellent, allowing to quickly estimate the Prugniel density profile as soon as the Sérsic parameters are known.